Supporting information for: Variable-temperature multinuclear solid-state NMR study of oxide ion dynamics in fluorite-type bismuth vanadate and phosphate solid electrolytes

Matthew T. Dunstan,[†,¶] David M. Halat,[†,¶] Matthew L. Tate,[‡] Ivana Radosavljevic Evans,[‡] and Clare P. Grey[*,†]

Department of Chemistry, University of Cambridge, Lensfield Road, Cambridge, CB2 1EW, United Kingdom, and Department of Chemistry, University Science Site, Durham University, South Road, Durham DH1 3LE, United Kingdom

E-mail: cpg27@cam.ac.uk

[*]To whom correspondence should be addressed

[†]Department of Chemistry, University of Cambridge, Lensfield Road, Cambridge, CB2 1EW, United Kingdom

[‡]Department of Chemistry, University Science Site, Durham University, South Road, Durham DH1 3LE, United Kingdom

[¶]Contributed equally to this work

XRD characterisation

Following ^{17}O-enrichment of the samples at 900°C, the phase purity was confirmed by powder XRD at room temperature (Figure S1).

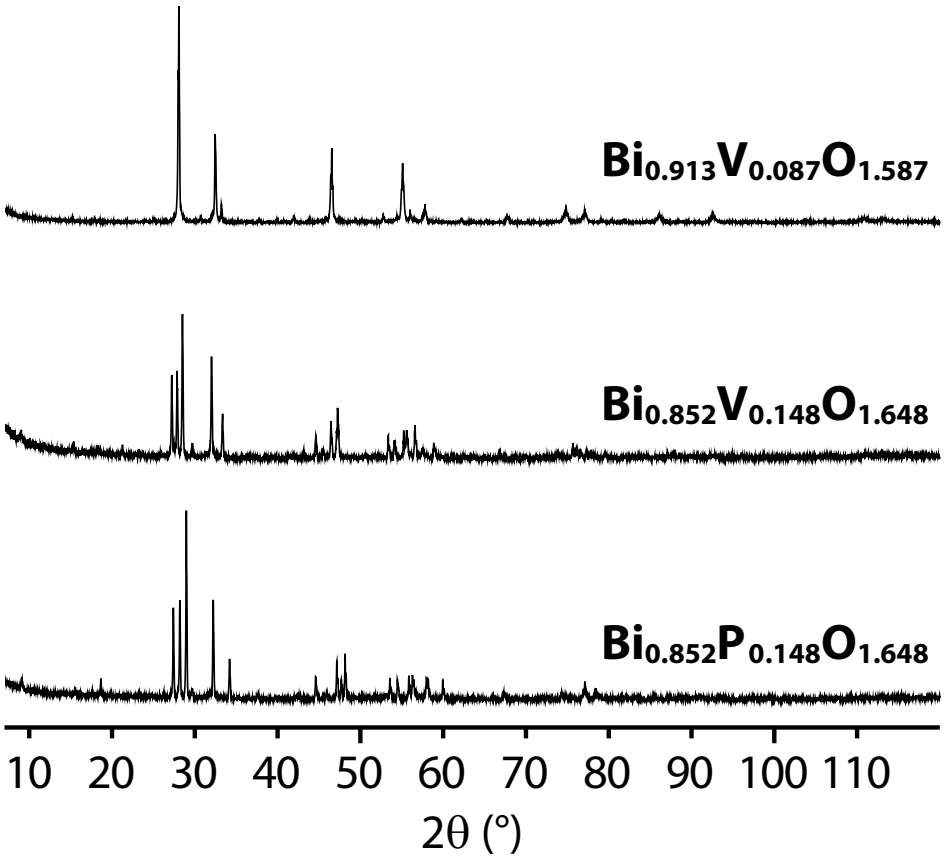


Figure S1: Ambient temperature powder XRD patterns of ^{17}O-enriched samples of $Bi_{0.913}V_{0.087}O_{1.587}$, $Bi_{0.852}V_{0.148}O_{1.648}$, and $Bi_{0.852}P_{0.148}O_{1.648}$. The patterns are in good agreement with those previously reported in the literature,[1,2] confirming that the samples remain phase-pure following the ^{17}O-enrichment procedure.

Complete VT-NMR datasets

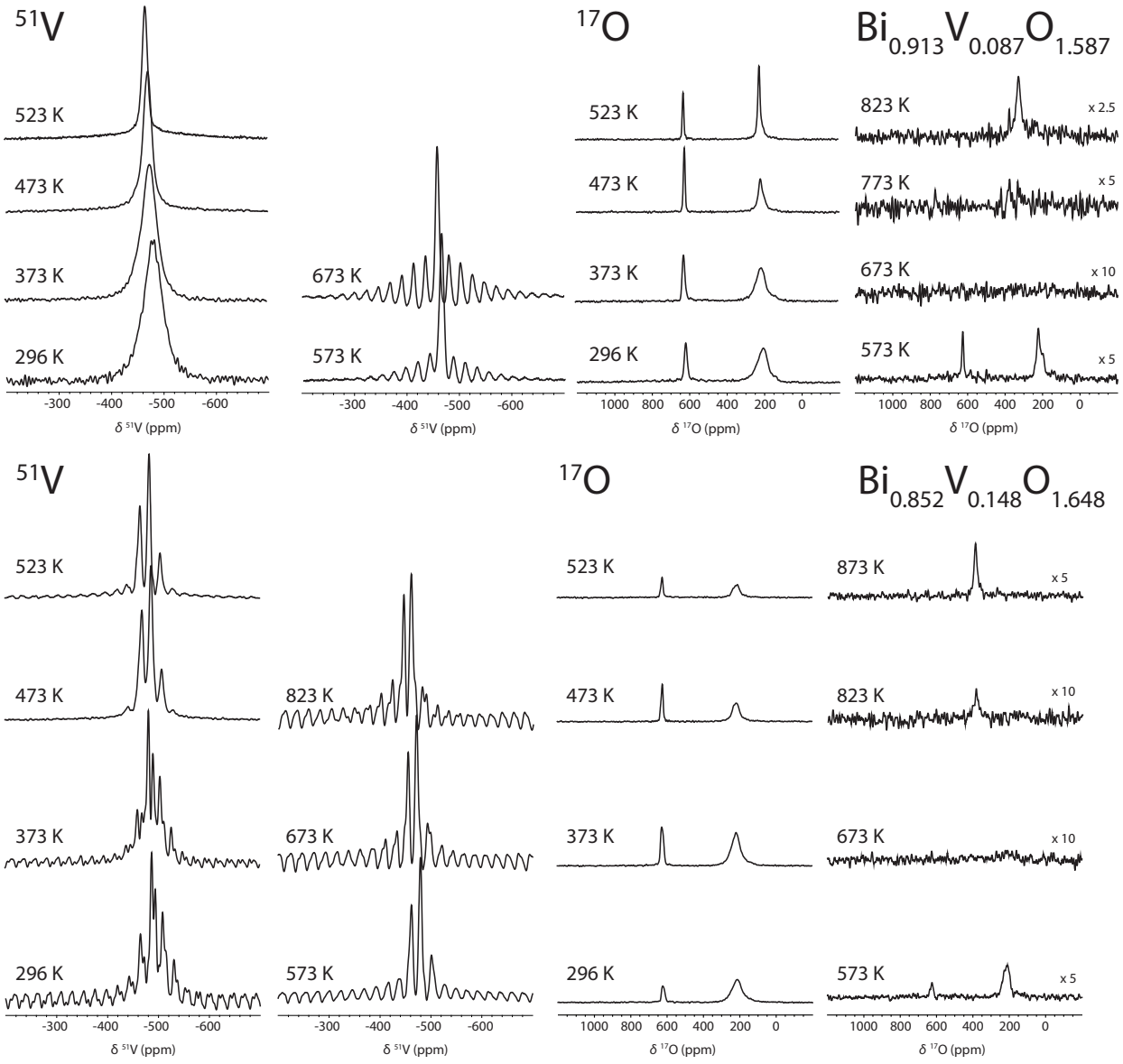


Figure S2: Full set of variable-temperature ^{17}O and ^{51}V NMR spectra of $Bi_{0.913}V_{0.087}O_{1.587}$ and $Bi_{0.852}V_{0.148}O_{1.648}$ obtained at 16.4 T at a spinning rate of 4 kHz, with recycle delays of 0.5 s and 50 ms for ^{51}V and ^{17}O, respectively. At room temperature, the centreband in the ^{51}V spectrum of $Bi_{0.913}V_{0.087}O_{1.587}$ is already broadened, indicating significant motion involving the O^V environment, whereas the corresponding spectrum of $Bi_{0.852}V_{0.148}O_{1.648}$ indicates slower motion, relative to the spinning frequency (4 kHz). The ^{17}O spectra for both V-substituted samples show the coalescence of the two distinct ^{17}O features at higher temperatures, indicative of increasingly fast oxide-ion motion and exchange between the sublattices with increasing temperature.

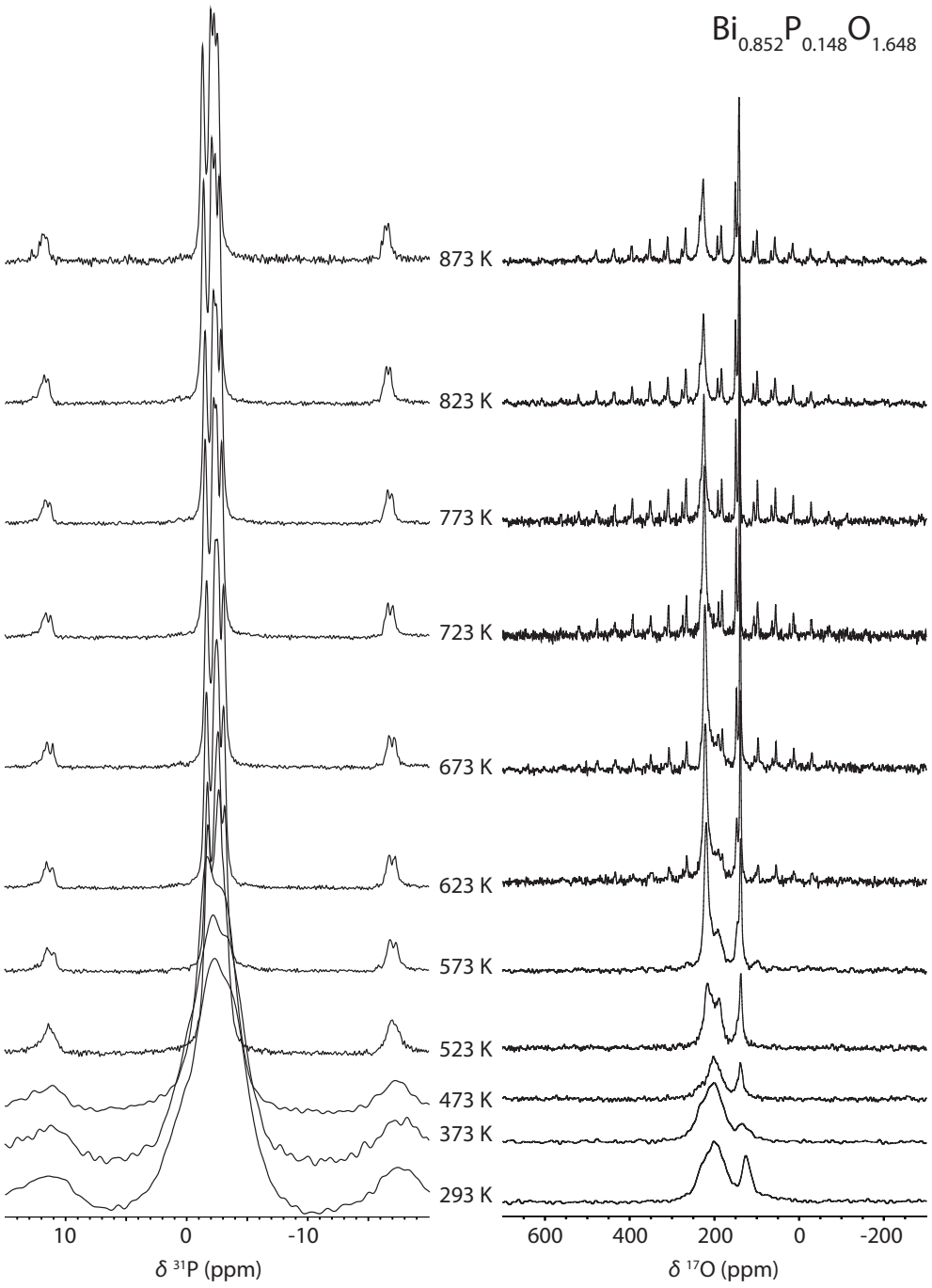


Figure S3: Full set of variable-temperature ^{31}P and ^{17}O NMR spectra of $Bi_{0.852}P_{0.148}O_{1.648}$ obtained at 16.4 T at a spinning rate of 4 kHz, with recycle delays of 30 s and 50 ms for ^{31}P and ^{17}O, respectively. The narrowing of the primary ^{31}P resonance is ascribed to nearby oxygen motion leading to motionally averaged local environments. At high temperature, four ^{31}P resonances are observed, in good agreement with the four crystallographically distinct environments reported in this material.[3] The O^{Bi} and O^{P} features in the ^{17}O NMR spectra remain distinct at higher temperatures, suggesting that motion remains confined to each sublattice, with sublattice exchange slower than the NMR timescale.

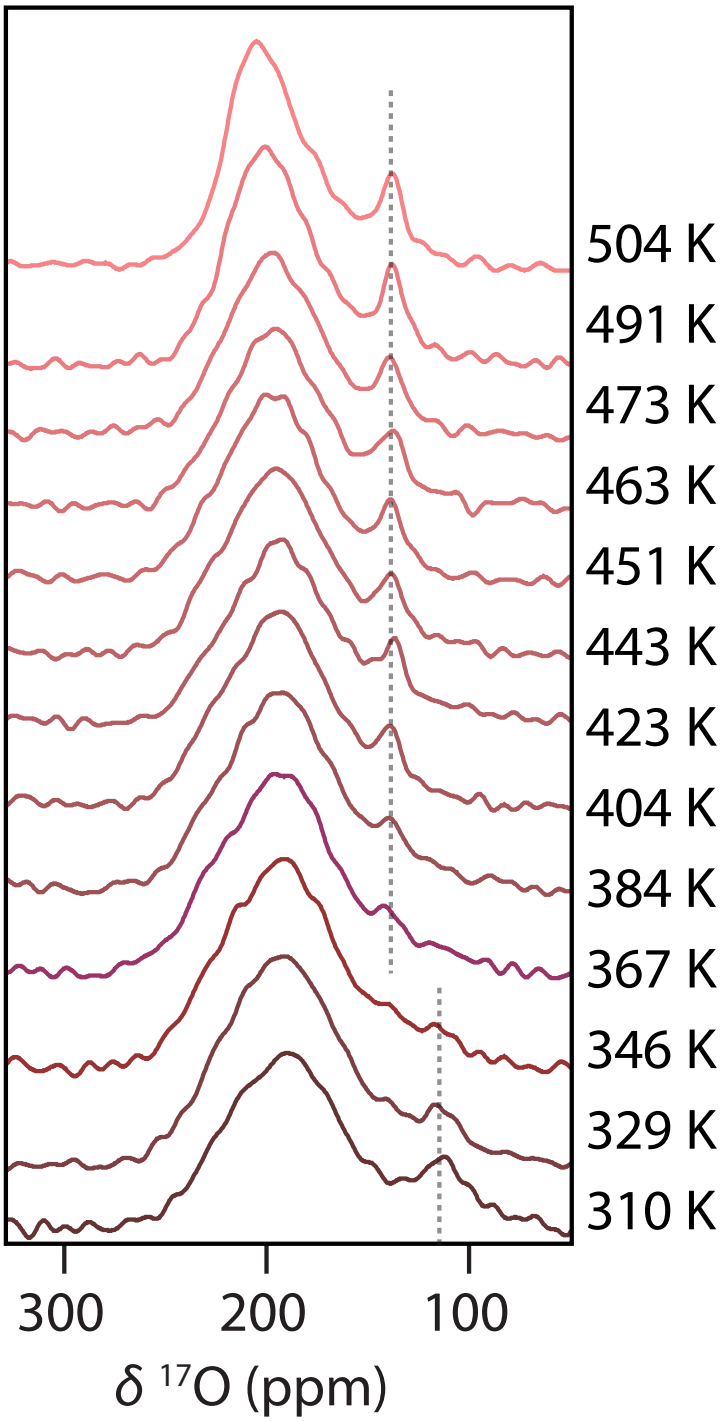


Figure S4: Variable-temperature ^{17}O NMR spectra of $Bi_{0.852}P_{0.148}O_{1.648}$, measured at 11.7 T at a spinning rate of 12.5 kHz, at 310–504 K. The dashed lines track the approximate temperature dependence of the shifts of the resonance arising from the O^P ^{17}O environment. With increasing temperature, this resonance first broadens, and then reappears above ∼367 K with a different ^{17}O chemical shift and further narrows at higher temperature, tentatively arising from localised exchange with another O^P environment overlapping with the more intense O^{Bi} peak.

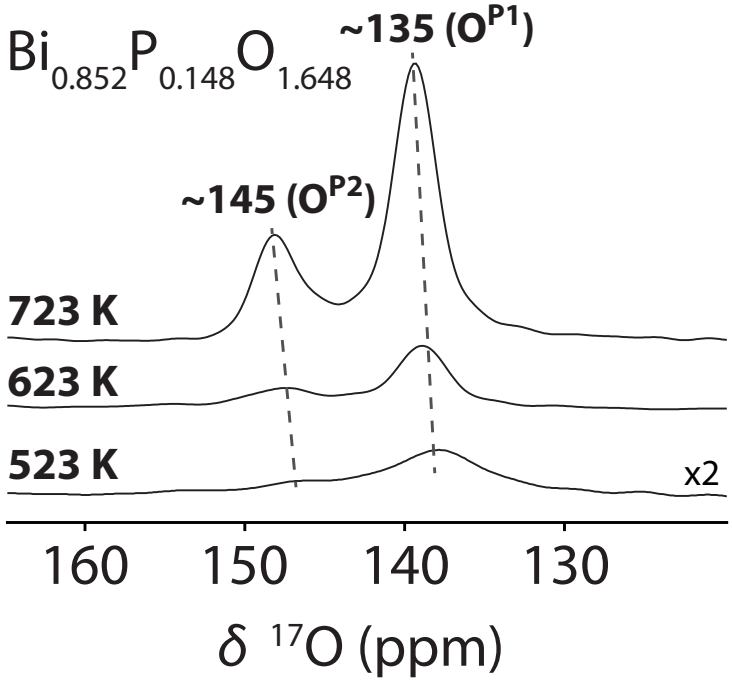


Figure S5: ^{17}O NMR spectra of $Bi_{0.852}P_{0.148}O_{1.648}$, focusing on the isotropic peaks of the O^P environments. Spectra were measured at 16.4 T and a spinning rate of 4 kHz, at 523–723 K. At temperatures $\leq$423 K, only one resonance is seen at $\sim$135 ppm which is fitted to a single Voigt peak. With increasing temperatures, a second resonance appears at $\sim$145 ppm and its intensity increases. The higher- and lower-frequency sites are assigned to O in differently distorted tetrahedral environments, respectively, with an intensity ratio of $\sim$1:3 as expected from crystallography.[3] The dashed lines track the approximate temperature dependence of the shifts of the two resonances.

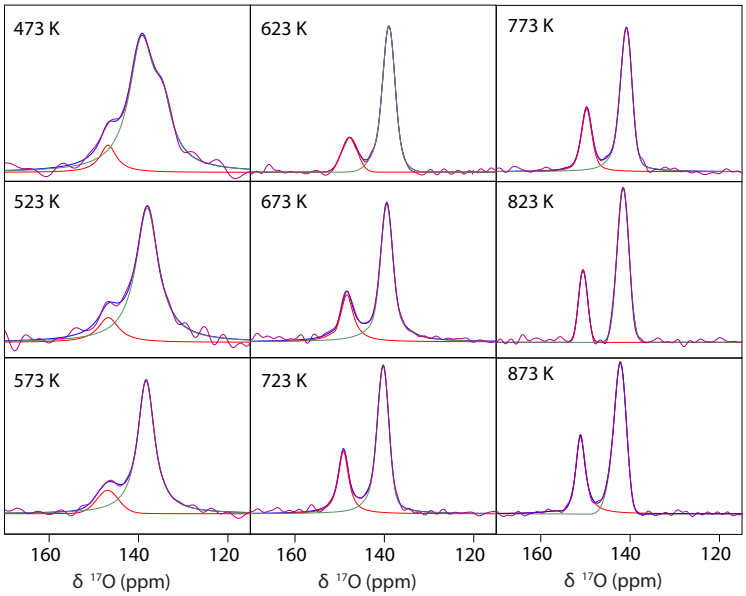


Figure S6: Variable-temperature ^{17}O NMR spectra of $Bi_{0.852}P_{0.148}O_{1.648}$, focusing on the isotropic peaks of the O^P environments, measured at 16.4 T at a spinning rate of 4 kHz from 473 K to 873 K. The O^P resonance in the $Bi_{0.852}P_{0.148}O_{1.648}$ sample comprises two distinct Voigt functions, with relative intensity changing with increasing temperature (compared to the single peak seen in $Bi_{0.913}V_{0.087}O_{1.587}$). Experimental spectra are shown in blue, summed fits in purple, and the individual fitted lineshapes in red and green respectively.

Faster MAS ^{51}V spectra of $Bi_{0.852}V_{0.148}O_{1.648}$

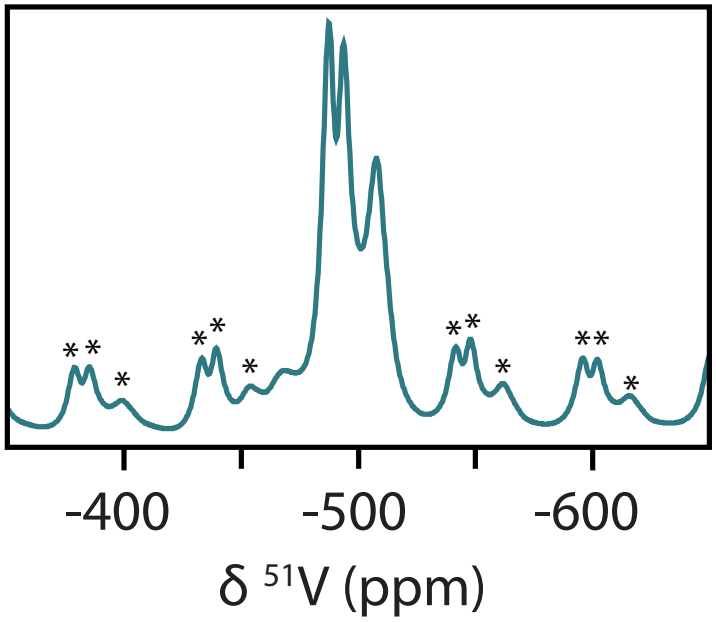


Figure S7: Room temperature ^{51}V NMR spectra of $Bi_{0.852}V_{0.148}O_{1.648}$, measured at 16.4 T at a spinning rate of 10 kHz. With this higher resolution, three major distinct V environments are discernible at −487, −493 and −508 ppm; a possible fourth environment is also present at −468 ppm. Asterisks denote spinning sidebands.

Fitting of ^{17}O quadrupolar parameters

The observed experimental NMR shift (in ppm) of a quadrupolar nucleus is in general field-dependent, due to the effect of the second-order quadrupolar interaction on the frequency of the central transition, *viz.*

$$\delta_{exp} = \delta_{CS} - \frac{1}{30} \cdot \left(1 + \frac{1}{3}\eta_Q^2\right) \cdot \left[I(I+1) - \frac{3}{4}\right] \cdot \left[\frac{3C_Q}{2I(2I-1)\,\omega_0}\right]^2, \quad (1)$$

where δ_{exp} is the observed experimental shift, δ_{CS} is the true chemical shift in the absence of the quadrupolar perturbation (*i.e.*, in the limit of infinite magnetic field), I is the nuclear spin ($5/2$ for ^{17}O), ω_0 is the Larmor frequency, and C_Q and η_Q are the quadrupolar coupling constant and asymmetry parameter, respectively.[4] By measuring δ_{exp} as a function of the ^{17}O Larmor frequency ω_0 by performing experiments at different magnetic fields, the slope of the best-fit line to δ_{exp} vs. ω_0^{-2} is seen to be directly proportional to the constant $C_Q^2 \cdot \left(1 + \frac{\eta_Q^2}{3}\right)$. Such a series of measurements at variable field has been performed for the O^{Bi} resonance in all studied samples (Figure S8); this gives values of $C_Q^2 \cdot \left(1 + \frac{\eta_Q^2}{3}\right)$ equal to 5.9 MHz^2 for $Bi_{0.913}V_{0.087}O_{1.587}$, 7.2 MHz^2 for $Bi_{0.852}V_{0.148}O_{1.648}$, and 8.0 MHz^2 for $Bi_{0.852}P_{0.148}O_{1.648}$. As the fits to the T_1 data only depend on this constant, and not the explicit values of C_Q and η_Q, we have not reported the latter and in fact cannot independently calculate them. However, for completeness, depending on the value of η_Q (between 0 and 1), the possible C_Q values of the O^{Bi} site vary between 2.1 and 2.4 MHz for $Bi_{0.913}V_{0.087}O_{1.587}$, 2.3 and 2.7 MHz for $Bi_{0.852}V_{0.148}O_{1.648}$, and 2.5 and 2.8 MHz for $Bi_{0.852}P_{0.148}O_{1.648}$.

The experimental shifts of the O^V resonances in the V-substituted samples show only a weak dependence on the magnetic field strength (Figure S9), which allows for maximum C_Q values of 0.8 MHz for $Bi_{0.913}V_{0.087}O_{1.587}$ and 0.9 MHz for $Bi_{0.852}V_{0.148}O_{1.648}$ to be extracted. The inset of Figure S9 shows a second-order quadrupolar broadened lineshape for a C_Q value of 0.9 MHz and η_Q value equal to 0. The cusps of this lineshape are separated by $\sim$0.5 ppm, which is much smaller than the $\sim$15 ppm difference observed between the two O^V features in the ^{17}O spectra of

$Bi_{0.852}V_{0.148}O_{1.648}$. The lineshapes of the O^V resonances in $Bi_{0.852}V_{0.148}O_{1.648}$ therefore do not result from the second-order quadrupolar interaction. The features are assigned to two distinct environments.

A similar analysis for the O^P resonance in the P-substituted $Bi_{0.852}P_{0.148}O_{1.648}$ sample, which also exhibits essentially no dependence on the magnetic field strength within error, allows an upper bound on the C_Q value equal to 0.6 MHz to be determined (Figure S10).

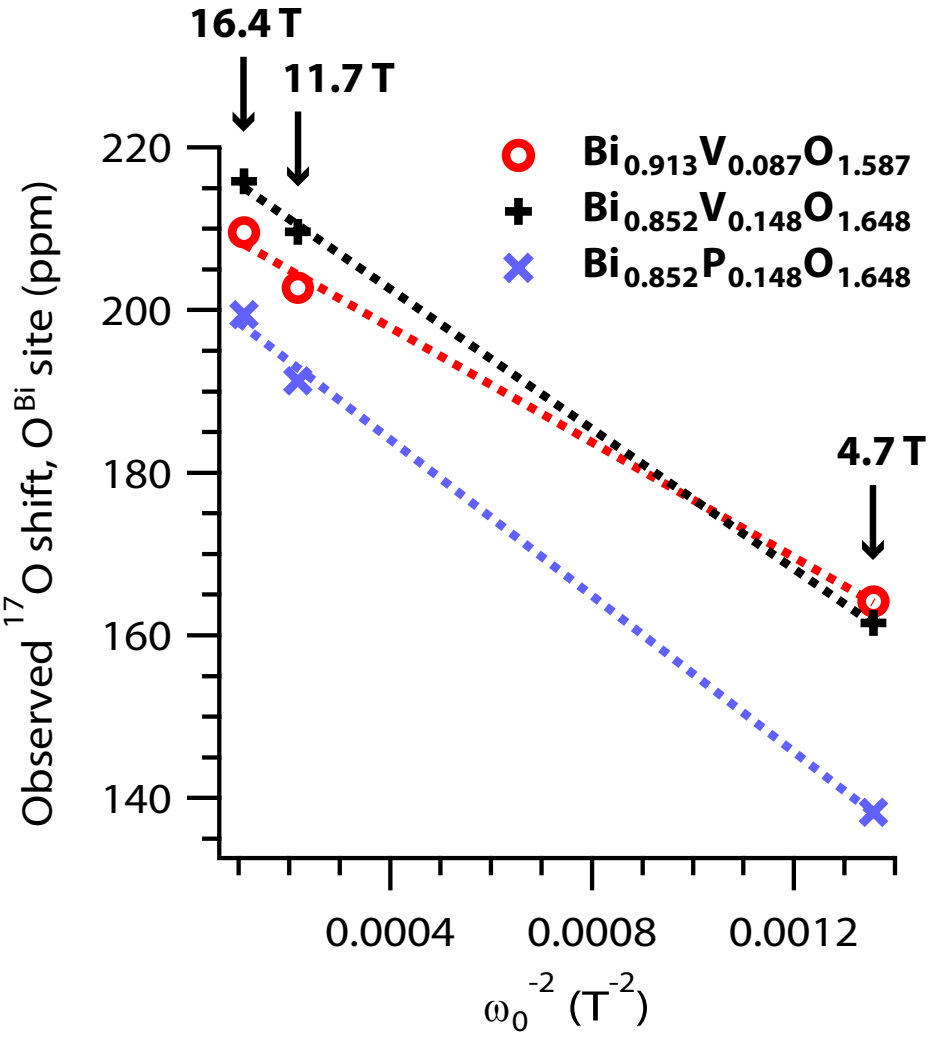


Figure S8: The observed ^{17}O chemical shift of the O^{Bi} feature for all three V- and P-substituted samples (at room temperature), as a function of the Larmor frequency ω_0 for ^{17}O; the experimental magnetic field is also indicated above each set of points. The slope of the best-fit lines (depicted as dotted lines) has then been used to extract the relevant proportionality constant $C_Q^2 \cdot \left(1 + \frac{\eta_Q^2}{3}\right)$ using the above equation.

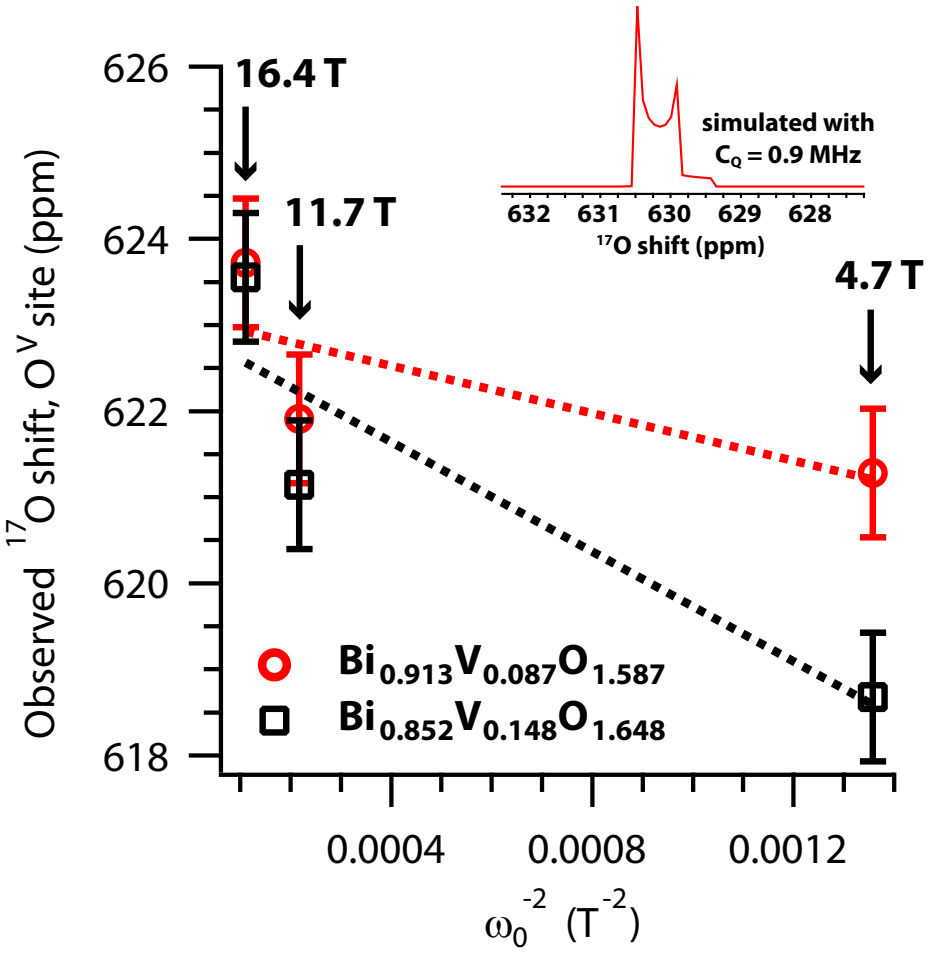


Figure S9: The observed ^{17}O chemical shift of the O^V feature for the V-substituted samples (at room temperature), as a function of the Larmor frequency ω_0 for ^{17}O; the experimental magnetic field is also indicated above each pair of points. (In the case of two features appearing in the spectra, as for $Bi_{0.852}V_{0.148}O_{1.648}$, the weighted average of the shifts of the two features is plotted.) The slope of the best-fit lines (depicted as dotted lines) has then been used to obtain upper bounds on the C_Q values of 0.8 MHz and 0.9 MHz for $Bi_{0.913}V_{0.087}O_{1.587}$ and $Bi_{0.852}V_{0.148}O_{1.648}$, respectively. Here, the fitting procedure is used only to bound the maximum size of the C_Q and the poor fit to the data is indicative of a very small C_Q. The inset shows the expected lineshape due to second-order quadrupolar broadening (at 16.4 T) in the case of C_Q = 0.9 MHz and η_Q = 0, which spans approximately 0.5 ppm.

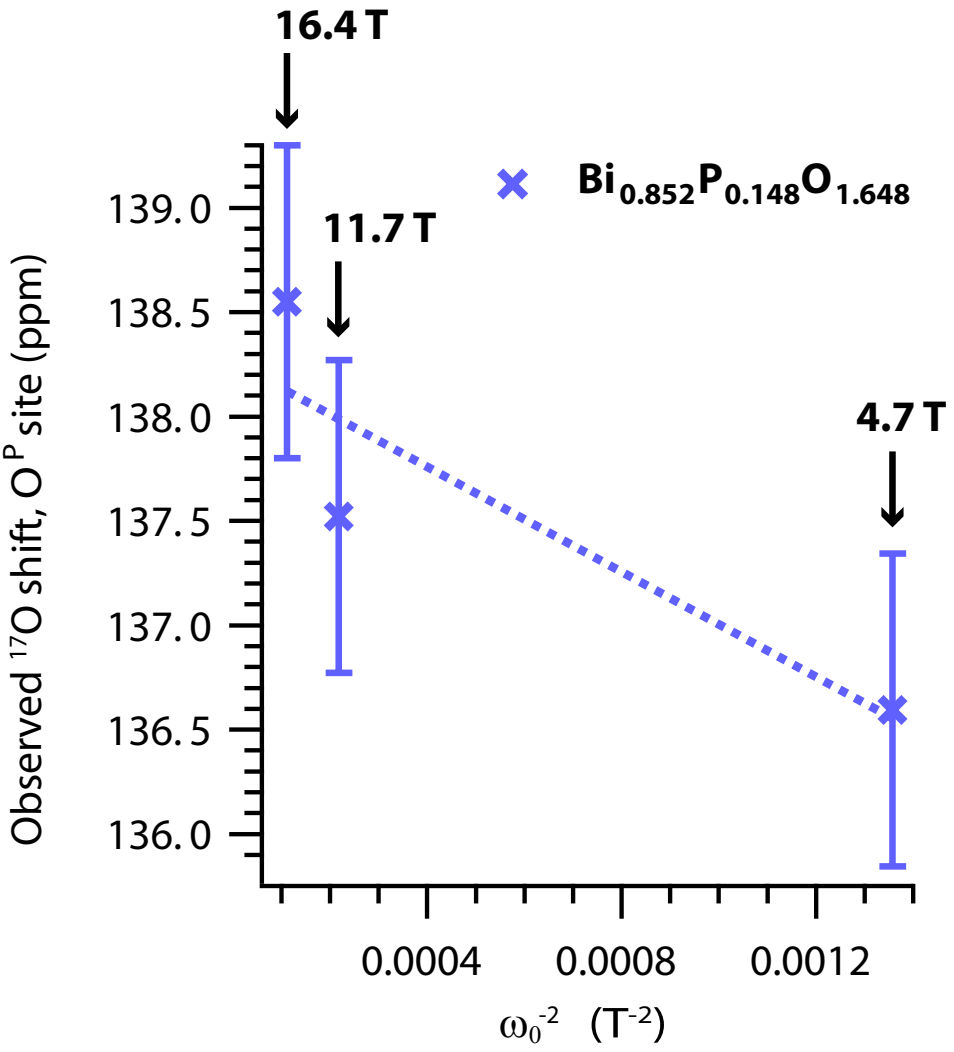


Figure S10: The observed ^{17}O chemical shift of the O^{P} feature for the P-substituted sample (at room temperature), as a function of the Larmor frequency ω_0 for ^{17}O; the experimental magnetic field is also indicated above each point. The slope of the best-fit line (depicted as a dotted line) has then been used to obtain an upper bound on the C_Q value of 0.6 MHz. Here, the fitting procedure is used only to bound the maximum size of the C_Q and the poor fit to the data is indicative of a very small C_Q.

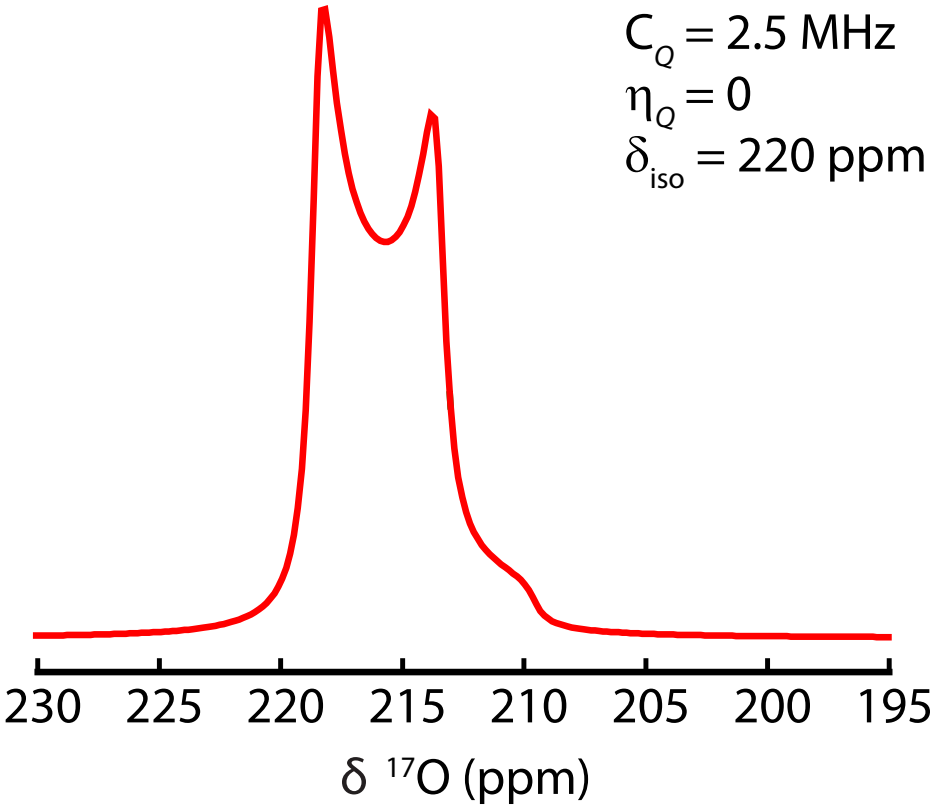


Figure S11: A simulated ^{17}O NMR spectrum assuming an isotropic shift of 220 ppm, C_Q value of 2.5 MHz, and $\eta_Q = 0$. The isotropic shift and quadrupolar parameters are taken from experimental data on the O^{Bi} environment in $Bi_{0.852}P_{0.148}O_{1.648}$. However, the spacing between the maxima of this simulated second-order quadrupolar lineshape is less than 10 ppm. In the experimental VT spectra recorded at 523 to 673 K (Fig 3 in the main text) two O^{Bi} peaks are resolved, with a separation of 20 to 30 ppm; as this is larger than the possible separation due to second-order quadrupolar effects, we discount the quadrupolar mechanism and assume that the two peaks correspond to distinct O^{Bi} sites.

Variable-temperature ^{17}O spectra of $Bi_{0.852}P_{0.148}O_{1.648}$ from saturation recovery (T_1) experiments

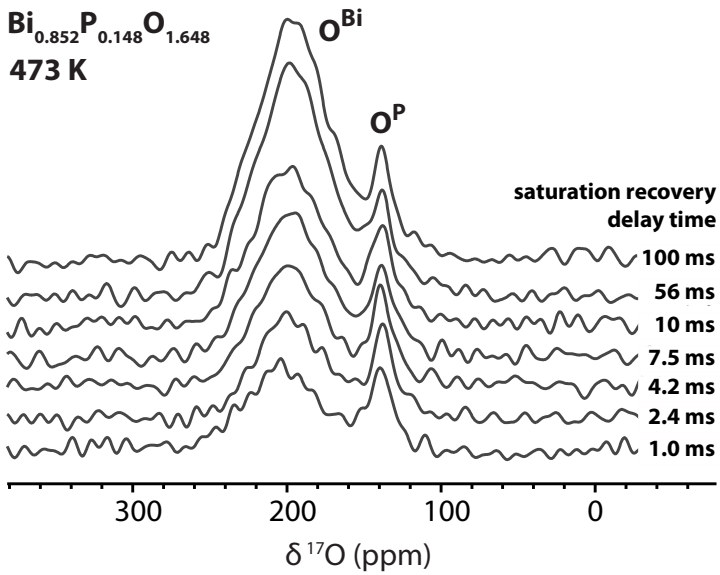


Figure S12: ^{17}O NMR spectra of $Bi_{0.852}P_{0.148}O_{1.648}$, measured at 11.7 T at a spinning rate of 12.5 kHz at a representative temperature of 473 K with different delay times in the saturation recovery measurement. The O^P environment appears to have a short, temperature-invariant T_1 value of $\sim$1 ms as shown by the relatively constant intensity of the corresponding peak.

^{17}O CT linewidths of O^{Bi} environments

This complex behaviour seen in the ^{17}O CT linewidths of O^{Bi} environments may tentatively arise from multiple motional mechanisms in the Bi–O sublattice operating across the same temperature range, such as local vacancy motion, long-range oxide-ion displacements, and/or the onset of sublattice exchange. Kuang *et al.* have also suggested multiple migration mechanisms occurring specifically within the Bi–O sublattice in the V-substituted materials, based on their AIMD results.[5]

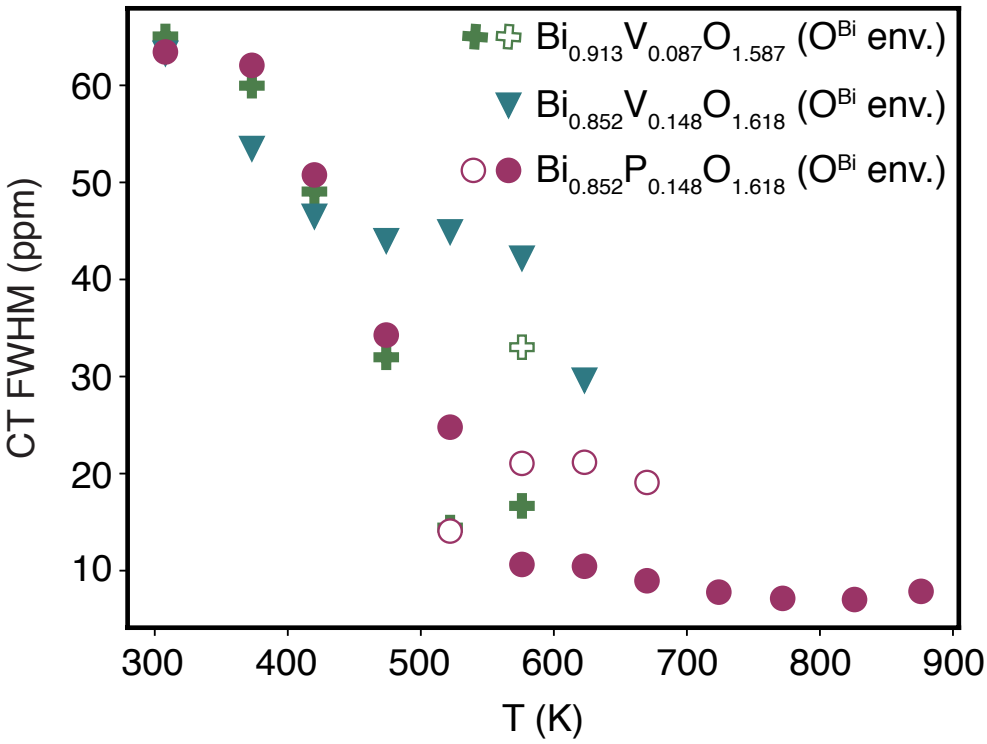


Figure S13: ^{17}O NMR CT full width at half maximum (FWHM) linewidths of the O^{Bi} environment in $Bi_{0.913}V_{0.087}O_{1.587}$, $Bi_{0.852}V_{0.148}O_{1.648}$ and $Bi_{0.852}P_{0.148}O_{1.648}$ plotted against temperature. The linewidth of both resonances narrows with increasing temperature, indicative of increasing rates of motion. At 573 K just before coalescence a second O^{Bi} environment is able to be measured in $Bi_{0.913}V_{0.087}O_{1.587}$ (open cross); however, no temperature-dependent trend can be ascertained. At higher temperatures, the O^{Bi} environment for for $Bi_{0.852}P_{0.148}O_{1.648}$ splits into two separate peaks (as discussed in the main text), which then coalesce at higher temperatures (full and open circles).

References

(1) Watanabe, A. Bi23M4O44.5 (M = P and V): New Oxide-Ion Conductors with Triclinic Structure Based on a Pseudo-Fcc Subcell. *Solid State Ionics* **1997**, *96*, 75–81.

(2) Kuang, X.; Payne, J. L.; Johnson, M. R.; Radosavljevic Evans, I. Remarkably High Oxide Ion Conductivity at Low Temperature in an Ordered Fluorite-Type Superstructure. *Angew. Chem.* **2012**, *51*, 690–694.

(3) Darriet, J.; Launay, J. C.; Zúniga, F. J. Crystal Structures of the Ionic Conductors Bi46M8O89 (M=P, V) Related to the Fluorite-Type Structure. *Journal of Solid State Chemistry* **2005**, *178*, 1753–1764.

(4) Man, P. P. Quadrupolar Interactions. In *Encyclopedia of Magnetic Resonance*; Harris, K. R., Wasylishen, R. E., Eds.; John Wiley & Sons, Ltd: Chichester, UK, 2011.

(5) Kuang, X.; Payne, J. L.; Farrell, J. D.; Johnson, M. R.; Evans, I. R. Polymorphism and Oxide Ion Migration Pathways in Fluorite-Type Bismuth Vanadate, Bi46V8O89. *Chem. Mater.* **2012**, *24*, 2162–2167.